

NeuroLIP: Interpretable and Fair Cross-Modal Alignment of fMRI and Phenotypic Text

Yanting Yang^{1,2} and Xiaoxiao Li^{1,2}✉

¹ The University of British Columbia, Vancouver, BC V6T 1Z4, Canada
xiaoxiao.li@ece.ubc.ca

² Vector Institute, Toronto, ON M5G 0C6, Canada

Abstract. Integrating functional magnetic resonance imaging (fMRI) connectivity data with phenotypic textual descriptors (*e.g.*, disease label, demographic data) holds significant potential to advance our understanding of neurological conditions. However, existing cross-modal alignment methods often lack interpretability and risk introducing biases by encoding sensitive attributes together with diagnostic-related features. In this work, we propose NeuroLIP, a novel cross-modal contrastive learning framework. We introduce text token-conditioned attention (TTCA) and cross-modal alignment via localized tokens (CALT) to the brain region-level embeddings with each disease-related phenotypic token. It improves interpretability via token-level attention maps, revealing brain region-disease associations. To mitigate bias, we propose a loss for sensitive attribute disentanglement that maximizes the attention distance between disease tokens and sensitive attribute tokens, reducing unintended correlations in downstream predictions. Additionally, we incorporate a negative gradient technique that reverses the sign of CALT loss on sensitive attributes, further discouraging the alignment of these features. Experiments on neuroimaging datasets (ABIDE and ADHD-200) demonstrate NeuroLIP’s superiority in terms of fairness metrics while maintaining the overall best standard metric performance. Qualitative visualization of attention maps highlights neuroanatomical patterns aligned with diagnostic characteristics, validated by the neuroscientific literature. Our work advances the development of transparent and fair neuroimaging AI.

1 Introduction

Neuroimaging research increasingly utilizes phenotypic text, such as diagnostic labels and demographic descriptors, as semantic anchors to understand functional connectivity patterns [11]. The integration of fMRI functional connectivity data with textual phenotypic descriptors offers significant potential to improve the prediction of neuropsychiatric disorders [10,16]. Advances in cross-modal contrastive learning (CMCL), notably CLIP [22] and SigLIP [29], have successfully aligned visual and textual representations. These methods use contrastive learning strategies to learn joint embedding spaces between images and their corresponding text descriptions by training image and text encoders for image-level and text-level representations, and then maximize similarity between paired

samples while minimizing similarity with negative pairs. Although these approaches have shown remarkable success in general computer vision tasks, their direct application to neuroimaging presents unique challenges, as they tend to obscure localized image-text relationships that are crucial for clinical interpretation, particularly in studying heterogeneous conditions like autism spectrum disorder (ASD), where associating brain regions with different text tokens is essential [13]. Moreover, CMCL in medical applications raises significant fairness concerns. Standard CMCL frameworks have been shown to inadvertently amplify demographic biases, such as encoding sex-related connectivity differences as proxies for psychiatric diagnoses [21]. Therefore, the direct application of the existing CMCL methods to neuroimaging and phenotypic descriptors encounters two main challenges: (1) limited fine-grained interpretability of cross-modal associations (*e.g.*, how text tokens are associated with brain regions) and (2) unintended demographic biases that conflate sensitive attributes with disease signatures [1].

Our work addresses these challenges by introducing a novel learning framework NeuroLIP that employs a *text token-conditioned attention* (TTCA) mechanism (Sec 2.2) and a *cross-model alignment via localized tokens* (CALT) strategy (Sec 2.3) that learns alignment between each brain region with each text token. Unlike prior approaches that treat interpretability and fairness separately, we propose their joint optimization through our text token attention and contrastive learning pipeline (Sec 2.4). Our innovative design achieves three key objectives: (1) developing an accurate neurodisorder classification model that utilizes both fMRI and phenotypic data; (2) mitigating bias by disentangling disease-related features from sensitive attributes using the TTCA module and a negative gradient loss approach in CALT; and (3) enhancing interpretability by localizing brain regions linked to disease prediction. We conduct comprehensive experiments on two independent neurodisorder datasets (ABIDE [ref] and ADHD-200 [ref]) to demonstrate our superior prediction performance and reduced bias among subgroups. Using attention map visualization and Neurosynth [28] meta-analytic maps for psychiatric phenotypes, we also offer neurally plausible explanations that were absent in previous CMCL methods.

2 Method

2.1 Overview of NeuroLIP and Notations

The overview of our proposed network is shown in Fig. 1. Given an atlas with N ROIs, we obtain the average time series data from the voxels within each ROI in the i -th fMRI image and calculate Pearson’s correlation coefficient (PCC) between time series of ROI pairs to measure connectivity, derived as $\mathbf{I}_i \in \mathbb{R}^{N \times N}$. The connectivity data \mathbf{I}_i is input into the vision model to obtain the brain node embeddings $\hat{\mathbf{I}}_i \in \mathbb{R}^{N \times N}$. To learn a better image representations, we use a multi-head self-attention (MHSA) layer, which takes brain node embeddings $\hat{\mathbf{I}}_i$ as key and value. For the query, we use a DEC module [27] to encode $\hat{\mathbf{I}}_i$ into $\tilde{\mathbf{I}}_i \in \mathbb{R}^{M \times N}$ and use $\tilde{\mathbf{I}}_i$ as input, which outputs the local image tokens

$\mathbf{v}_i^{\text{loc}} \in \mathbb{R}^{M \times N}$. The global image tokens $\mathbf{v}_i^{\text{g}} \in \mathbb{R}^N$ is pooled over DEC output $\tilde{\mathbf{I}}_i$. For the text input of the j -th image $\mathbf{T}_j \in \mathbb{R}^S$, where S is the text sequence length, the text data is input into the text model to obtain the local text tokens $\mathbf{t}_j^{\text{loc}} \in \mathbb{R}^{S \times N}$. The global text token $\mathbf{t}_j^{\text{g}} \in \mathbb{R}^N$ is pooled over local text tokens $\mathbf{t}_j^{\text{loc}}$. Subsequently, TTCA is employed for dynamic image feature selections such that $\mathbf{v}_{i,j}^{\text{ttca}} = f(\mathbf{t}_j^{\text{loc}}, \mathbf{v}_i^{\text{loc}})$ (detailed in Sec. 2.2). Finally, we apply the CALT loss $\mathcal{L}^{\text{calt}}$, incorporated with the negative gradient technique, for image-text feature alignment (detailed in Sec. 2.3) and attention loss $\mathcal{L}^{\text{attn}}$ for sensitive attributes debiasing (detailed in Sec. 2.4).

2.2 Text Token-Conditioned Attention

NeuroLIP aims to integrate both fMRI data and phenotypic information into a neurodisorder classification framework while simultaneously interpreting how brain region activities are associated with disease labels. To achieve this, we introduce a **Text Token-Conditioned Attention** (TTCA) mechanism that explicitly aligns individual brain region activations with corresponding phenotypic descriptors and disease labels. Most existing CMCL methods [22,29] lack this level of fidelity, as they typically represent the input image as a single global embedding, thereby losing regional specificity. Instead of encoding the entire fMRI scan into a single vector, we aim to preserve the fidelity of brain regions by maintaining their distinct representations. Inspired by the recent work FLAIR [26], which demonstrated that contextualizing local image representations with global text embeddings can enhance interpretability, we extend this idea further. Specifically, we preserve local image tokens $\mathbf{v}^{\text{loc}} \in \mathbb{R}^{M \times E}$, where M represents the number of brain regions and E is the embedding dimension, ensuring that each token corresponds to a distinct brain region. However, unlike FLAIR [26], which aligns image features with a global text embedding, we retain token-wise text representations $\mathbf{t}^{\text{loc}} \in \mathbb{R}^{S \times E}$, where S is the number of text tokens. This modification enables the formation of localized image-text token pairs, where each brain region’s activation is explicitly associated with a

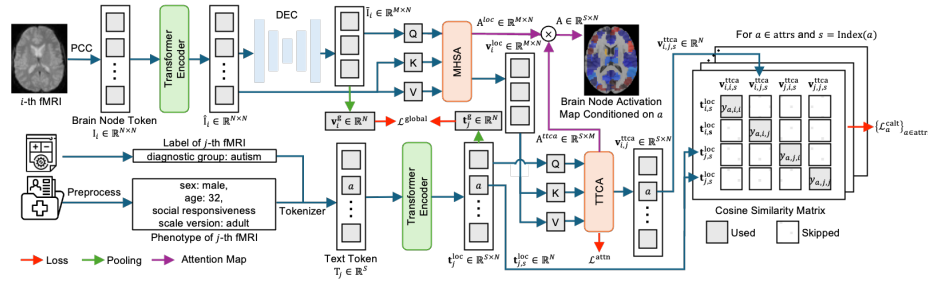


Fig. 1. Overview of NeuroLIP. Here, we show the pipeline applied on a batch of two (i -th and j -th) fMRI images and we present the interaction between the i -th image and the phenotypic text of j -th image.

specific text token. With this enhancement, our TTCA allows us to extract image features that are dynamically conditioned on each individual text token, rather than a global representation. To effectively contextualize the image representation with local text tokens, we introduce an TTCA layer f , which produces text token-conditioned image representations \mathbf{v}^{ttca} from local image tokens \mathbf{t}^{loc} . We define it as

$$f(\mathbf{t}^{\text{loc}}, \mathbf{v}^{\text{loc}}) = \text{softmax} \left(\frac{\mathbf{t}^{\text{loc}} W_q (\mathbf{v}^{\text{loc}} W_k)^\top}{\sqrt{d}} \right) \mathbf{v}^{\text{loc}} W_v \quad (1)$$

where W_q, W_k, W_v are the query, key, and value projection matrices. In practice, we utilize a multi-head self-attention (MHSA) layer and append an empty token to \mathbf{v}^{loc} to allow \mathbf{t}^{loc} to attend to it when not semantically related to \mathbf{v}^{loc} .

The attention weights produced by the TTCA layer offer valuable insights into the interactions between local image tokens and local text tokens, enabling the visualization of activation maps that highlight how different textual elements influence specific regions of an image. In practice, we apply another MHSA layer to condition local image tokens on DEC outputs, denoting attention weight matrices from TTCA and MHSA layer as $\mathbf{A}^{\text{loc}} \in \mathbb{R}^{M \times N}$ and $\mathbf{A}^{\text{ttca}} \in \mathbb{R}^{S \times M}$, respectively. Multiplying these gives the token-node attention matrix $\mathbf{A} \in \mathbb{R}^{S \times N}$. Each element $A_{s,n}$ in \mathbf{A} represents the attention weight between the s -th text and the n -th brain node, quantifying each brain region’s relevance to a specific text descriptor. To visualize the activation map for a text token at index s , extract the corresponding attention weights across all brain regions:

$$\mathbf{A}_s = \{A_{s,1}, A_{s,2}, \dots, A_{s,N}\} \quad (2)$$

which can then be overlaid on the image to highlight regions that are most responsive to the text token s . This visualization facilitates the interpretation of cross-modal alignment by revealing which parts of the brain are activated by specific textual information. Moreover, by analyzing these activation maps across different text tokens, we can identify patterns of hypoconnectivity, where certain image regions exhibit consistently low attention weights in response to particular types of text tokens. Such patterns may indicate areas of the image that are less semantically aligned with the corresponding textual descriptions, potentially uncovering underlying structures or attributes that are not prominently captured by the model. Eq. (2) demonstrates how localized attention quantifies interdependencies between image and text tokens. By leveraging these attention weights for visualization, we gain a deeper understanding of the model’s interpretability, enabling the identification of meaningful cross-modal relationships and highlighting potential areas of improvement in the alignment process.

2.3 Cross-Modal Alignment via Localized Tokens

We begin by considering the cosine similarity matrix between image and text embeddings, where positive pair is represented as $\langle \mathbf{v}_i^{\text{g}}, \mathbf{t}_i^{\text{g}} \rangle$ and the negative pair

as $\langle \mathbf{v}_i^g, \mathbf{t}_j^g \rangle$, with $i \neq j$. The alignment process is guided by a sigmoid loss function [29], denoted as $\mathcal{L}^{\text{global}}$. Let s denote the index of attribute a within the text sequence, encompassing sensitive, non-sensitive attribute, and disease label. By employing TTCA (Sec 2.2), we expand the scope of image-text pairs to image-text local token pairs. Therefore, the positive pair becomes $\langle \mathbf{v}_{i,i,s}^{\text{ttca}}, \mathbf{t}_{i,s}^{\text{loc}} \rangle$, while the negative pairs are $\langle \mathbf{v}_{i,j,s}^{\text{ttca}}, \mathbf{t}_{i,s}^{\text{loc}} \rangle$, $\langle \mathbf{v}_{i,j,s}^{\text{ttca}}, \mathbf{t}_{j,s}^{\text{loc}} \rangle$, and $\langle \mathbf{v}_{i,j,s}^{\text{ttca}}, \mathbf{t}_{k,s}^{\text{loc}} \rangle$, where $\mathbf{v}_{i,j,s}^{\text{ttca}}$ is the image embedding from the i -th image conditioned on the s -th text token of image j , $\mathbf{t}_{i,s}^{\text{loc}}$ is the s -th local text tokens of image i , and $i \neq j \wedge i \neq k$. For simplicity, we omit negative pairs related to different tokens. Previous study [26] shows that only the pair $\langle \mathbf{v}_{i,j,s}^{\text{ttca}}, \mathbf{t}_{j,s}^{\text{loc}} \rangle$ significantly contributes to effective image-text alignment, allowing us to disregard the other two types of negative pairs to reduce computational costs. The utilization of localized text tokens increases the likelihood that identical text tokens are shared across multiple images, particularly for categorical attributes. Consequently, for each attribute a , we construct the labels \mathbf{y} as

$$y_{a,i,j} = 2 \cdot \mathbb{1}(G_{a,i} = G_{a,j}) - 1 \quad (3)$$

where $y_{a,i,j}$ is the label for the pair $\langle \mathbf{v}_{i,j,s}^{\text{ttca}}, \mathbf{t}_{j,s}^{\text{loc}} \rangle$, $\mathbb{1}$ denotes the indicator function and $G_{a,i}$ represents the ground truth of attribute a for image i . With positive / negative pairs and labels, we define our **Cross-Modal Alignment via Localized Tokens** (CALT) loss as

$$\mathcal{L}_{a,i,j}^{\text{calt}} = \frac{1}{1 + e^{y_{a,i,j}(-t \langle \mathbf{v}_{i,j,s}^{\text{ttca}}, \mathbf{t}_{j,s}^{\text{loc}} \rangle)}}, \quad (4)$$

where s is the index of attribute a and t is a learnable weight. To incorporate the negative gradient technique, we can simply reverse the sign of this sigmoid loss, enforcing the unalignment of the sensitive attribute.

2.4 Sensitive Attribute Disentanglement

In the analysis of medical images and text, it is essential to distinguish between disease-related information and sensitive attributes, such as sex or age, to prevent the model from inadvertently learning or propagating biases associated with these attributes. To achieve this, we propose maximizing the distance between the attention weights related to disease tokens and those associated with sensitive demographic tokens. This encourages the model to treat these two types of information as distinct, thereby reducing bias. As detailed in Sec. 2.2, the attention weight from the local text token-conditioned attention pooling layer signifies the interaction between local text tokens at position s and local image tokens. We identify and isolate sensitive attributes by extracting the corresponding attention weights at their positions, denoted as $\mathbf{A}_{\text{disease}}^{\text{ttca}}$ and $\mathbf{A}_{\text{sensitive}}^{\text{ttca}}$. The attention loss can then be defined as

$$\mathcal{L}^{\text{attn}} = \|\mathbf{A}_{\text{disease}}^{\text{ttca}} - \mathbf{A}_{\text{sensitive}}^{\text{ttca}}\|_2 \quad (5)$$

where the L2 norm (Euclidean distance) is used to calculate this distance. The overall loss function \mathcal{L} integrates the attention loss $\mathcal{L}^{\text{attn}}$ designed to maximize

the aforementioned distance, in addition to the CALT loss $\mathcal{L}^{\text{calt}}$ that ensure image-text alignment, and a global loss $\mathcal{L}^{\text{global}}$. The implementation involves optimizing this joint loss function during training:

$$\mathcal{L} = \mathcal{L}^{\text{global}} + \sum_a^{\text{attrs}} \text{sign}(a) \mathcal{L}_a^{\text{calt}} - \beta \mathcal{L}^{\text{attn}}, \quad (6)$$

where $\text{sign}(a) = 1$ for sensitive attributes and 1 otherwise. β is a hyperparameter.

3 Experiments and Results

3.1 Experimental Setup

Datasets: We used two publicly available resting state fMRI datasets: ABIDE [9] and ADHD-200 [2]. For ABIDE, we used data processed by the C-PAC pipeline [6] and that passed quality assessments, resulting in 403 individuals with ASD and 468 controls. For ADHD-200, we used data processed by the Athena pipeline [4], excluding images lacking phenotypic information, which produced 356 individuals with Attention-Deficit / Hyperactivity Disorder (ADHD) and 582 controls. Multiple individual scans resulted in 525 ADHD images and 842 control images. In both datasets, signals were bandpass filtered without global signal regression, and functional connectivity matrices were defined using the Craddock 200 atlas [7]. Phenotypic text was formatted as “diagnostic group: {dx_group}, sex: {sex}, age: {age}, social responsiveness scale version: {srs},” where {dx_group}, {sex}, and {srs} are categorical, and {age} is rounded to the nearest integer. The {srs} value, either child or adult, is determined by whether {age} is below or above 18. We select {srs} as the sensitive attribute for ABIDE dataset and {sex} for ADHD-200 dataset. All other attributes are viewed as normal attribute.

Metrics: For *classification performance*, we use Area Under the Receiver Operating Characteristic Curve (AUC), Accuracy (ACC), Sensitivity (SEN), Specificity (SPC). For *fairness*, we use Demographic Parity Difference (DPD) [3], Difference in Equalized Odds (DEOdds) [3], Equity-Scaled AUC [20].

Training Setup: We utilize the AdamW [18] optimizer with 1×10^{-4} initial learning rate, 1×10^{-4} weight decay, 32 batch size and 64 epoches. We use a cosine scheduler with a 3% warmup ratio. We retain 20% of the ABIDE data and the original ADHD-200 test release ($\approx 12.5\%$ of the data) as test set. We let $\beta = 0.001$ and implement a 5-fold cross-validation (CV) on the remaining training set for every experiment. All data split is implemented in a stratified manner based on the diagnostic group.

3.2 Experimental Results

Baseline Comparison: We first compare NeuroLIP with transformer-based fMRI classification model BrainNetTF [15] supervised trained using disease label and CMCL baselines, including CLIP [22], SigLIP [29], and FairCLIP [19], a fair learning method using Sinkhorn distance to align the visual-text feature

Table 1. Comparison with baseline methods. The best results are **bolded** and the second best results are underlined.

Method	ABIDE						
	AUC \uparrow	ACC \uparrow	SEN \uparrow	SPC \uparrow	DPD \downarrow	DEOdds \downarrow	ES-AUC \uparrow
BrainNetTF	71.69	66.74	62.22	70.64	13.12	21.40	69.04
CLIP	71.15	66.51	61.73	<u>70.64</u>	15.60	22.92	<u>67.77</u>
SigLIP	71.88	67.77	64.20	70.85	10.32	20.00	68.96
FairCLIP	<u>71.09</u>	67.09	67.90	66.38	11.60	19.12	66.82
NeuroLIP (ours)	72.43	<u>66.29</u>	64.69	67.66	7.92	16.70	70.00
Method	ADHD-200						
	AUC \uparrow	ACC \uparrow	SEN \uparrow	SPC \uparrow	DPD \downarrow	DEOdds \downarrow	ES-AUC \uparrow
BRAINNETTF	55.48	58.60	37.40	75.96	12.26	13.65	52.32
CLIP	59.12	59.18	<u>42.08</u>	73.19	11.65	11.73	56.26
SigLIP	59.97	60.82	42.34	75.96	9.88	10.49	57.63
FairCLIP	<u>57.98</u>	60.35	37.14	79.36	11.53	<u>10.85</u>	55.76
NeuroLIP (ours)	62.74	60.12	38.96	<u>77.45</u>	8.59	6.18	59.38

Table 2. The impact of each component of our proposed NeuroLIP. The best results are **bolded** and the second best results are underlined.

Component		ABIDE						
$\mathcal{L}^{\text{attn}}$	Neg. Grad.	AUC \uparrow	ACC \uparrow	SEN \uparrow	SPC \uparrow	DPD \downarrow	DEOdds \downarrow	ES-AUC \uparrow
\times	\times	<u>72.32</u>	67.66	62.47	72.13	11.60	18.54	68.77
\checkmark	\times	70.58	67.54	<u>63.21</u>	<u>71.28</u>	10.48	18.32	67.59
\times	\checkmark	72.10	68.11	64.69	71.06	9.36	18.28	69.90
\checkmark	\checkmark	72.43	<u>66.29</u>	64.69	67.66	7.92	16.70	70.00
Component		ADHD-200						
$\mathcal{L}^{\text{attn}}$	Neg. Grad.	AUC \uparrow	ACC \uparrow	SEN \uparrow	SPC \uparrow	DPD \downarrow	DEOdds \downarrow	ES-AUC \uparrow
\times	\times	59.08	58.36	36.10	76.60	9.26	12.34	54.93
\checkmark	\times	58.89	58.60	35.84	<u>77.23</u>	9.49	9.12	56.23
\times	\checkmark	60.71	<u>58.60</u>	47.01	68.09	7.85	8.22	58.79
\checkmark	\checkmark	62.74	60.12	38.96	77.45	8.59	6.18	59.38

similarities across demographic groups. As the mean value of 5-fold CV shown in Table 1, NeuroLIP consistently outperforms these baselines in all fairness measures while maintaining top classification performance.

Ablation Study: To understand the impact of each component in NeuroLIP, we conducted a series of ablation studies by systematically removing key elements of our approach. As presented in Table 2, we evaluate the effect of the attention loss ($\mathcal{L}^{\text{attn}}$) and the negative gradient (Neg. Grad.). The results indicate that both components contribute notably to the model’s ability to mitigate bias. Without the attention loss, the fairness metrics, such as DPD and DE-Odds, worsen, demonstrating its role in disentangling sensitive attributes from disease-related features. Similarly, the absence of the negative gradient technique results in higher bias, as indicated by increased fairness metrics, underscoring its importance in discouraging the alignment of sensitive attributes. The full implementation of NeuroLIP, combining both components, achieves the best balance between accuracy and fairness, confirming the synergistic effect of our proposed modifications in advancing fairness of neuroimaging analysis.

Interpretation: We visualize attention maps in Fig. 2 generated by our TTCA layer to illustrate how specific phenotypic descriptors modulate fMRI connectivity features. In both ABIDE and ADHD-200 datasets, these maps show distinct patterns when conditioned on diagnostic versus control tokens. In the ABIDE data set, autism-conditioned attention maps consistently highlight regions in the

superior parietal lobes, which are key to spatial attention and sensory integration, often show altered engagement during visuospatial tasks [8]. Additionally, regions like the right middle and superior occipital gyri, along with the right lingual gyrus, support the processing of complex visual stimuli and object recognition, and are implicated in the local processing biases seen in autism [14]. In the ADHD-200 datasets, the differential activation patterns in frontal operculum and middle frontal regions critical for inhibitory control and executive functions often show reduced activation during tasks requiring sustained attention [25]. Bilateral insular cortices, which contribute to salience detection and the integration of emotional and cognitive information, are frequently reported as dysfunctional in ADHD, with evidence of both hypo- and hyperactivation [17]. By comparing these maps against Neurosynth [28] meta-analytic results, we observed that the activated brain regions of patients with Autism have a stronger correlation to vision [24] and motion [12], while the activation map of patients with ADHD is more related to language [5] and recognition [23], indicating a strong correspondence between our model’s highlighted regions and those frequently reported in the literature. This agreement reinforces the clinical plausibility of our findings.

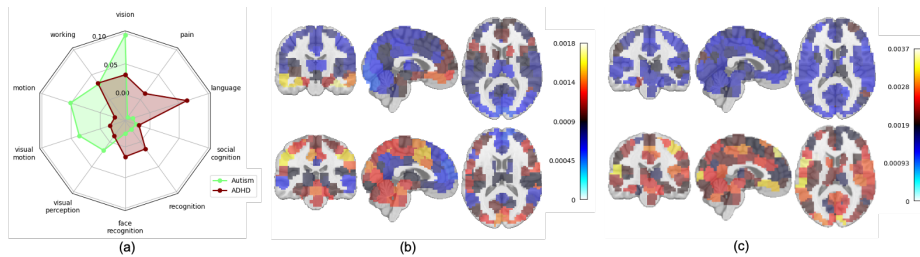


Fig. 2. (a) Meta-analysis. (b) Attention map conditioned on control (top) and ASD (bottom) in the ABIDE dataset. (c) Attention map conditioned on control (top) and ADHD (bottom) in the ADHD-200 dataset.

4 Conclusion

In this work, we introduced NeuroLIP, a novel framework for cross-modal alignment that integrates fMRI connectivity data with phenotypic text. NeuroLIP significantly mitigates demographic bias while maintaining or improving classification performance. By leveraging TTCA, NeuroLIP generates interpretable attention maps that uncover neuroanatomically meaningful patterns. These maps, validated against meta-analytic data, provide clinicians and researchers with transparent insights into the underlying brain region-disease associations. Furthermore, our incorporation of a sensitive attribute disentanglement loss and a negative gradient technique effectively discourages the inadvertent alignment of demographic features with disease labels, addressing a critical challenge in neuroimaging analysis. Future work will focus on extending NeuroLIP to larger and more diverse datasets.

References

1. Abbasi-Sureshjani, S., Raumanns, R., Michels, B.E., Schouten, G., Cheplygina, V.: Risk of training diagnostic algorithms on data with demographic bias. *Interpretable and Annotation-Efficient Learning for Medical Image Computing: Third International Workshop (2020)*
2. ADHD-200 consortium: The adhd-200 consortium: a model to advance the translational potential of neuroimaging in clinical neuroscience. *Frontiers in systems neuroscience (2012)*
3. Agarwal, A., Beygelzimer, A., Dudík, M., Langford, J., Wallach, H.M.: A reductions approach to fair classification. *International Conference on Machine Learning (2018)*
4. Bellec, P., Chu, C., Chouinard-Decorte, F., Benhajali, Y., Margulies, D.S., Craddock, R.C.: The neuro bureau adhd-200 preprocessed repository. *Neuroimage (2017)*
5. Cohen, N.J., Vallance, D.D., Barwick, M., Im, N., Menna, R., Horodezky, N.B., Isaacson, L.: The interface between adhd and language impairment: An examination of language, achievement, and cognitive processing. *Journal of child Psychology and Psychiatry (2000)*
6. Craddock, C., Sikka, S., Cheung, B., Khanuja, R., Ghosh, S.S., Yan, C., Li, Q., Lurie, D., Vogelstein, J., Burns, R., Colcombe, S., Mennes, M., Kelly, C., Di Martino, A., Castellanos, F.X., Milham, M.: Towards automated analysis of connectomes: The Configurable Pipeline for the Analysis of Connectomes (C-PAC). *Frontiers in Neuroinformatics (2013)*
7. Craddock, R.C., James, G.A., Holtzheimer III, P.E., Hu, X.P., Mayberg, H.S.: A whole brain fmri atlas generated via spatially constrained spectral clustering. *Human brain mapping (2012)*
8. DeRamus, T.P., Black, B.S., Pennick, M.R., Kana, R.K.: Enhanced parietal cortex activation during location detection in children with autism. *Journal of neurodevelopmental disorders (2014)*
9. Di Martino, A., Yan, C.G., Li, Q., Denio, E., Castellanos, F.X., Alaerts, K., Anderson, J.S., Assaf, M., Bookheimer, S.Y., Dapretto, M., et al.: The autism brain imaging data exchange: towards a large-scale evaluation of the intrinsic brain architecture in autism. *Molecular psychiatry (2014)*
10. Gao, Y., Shuai, D., Bu, X., Hu, X., Tang, S., Zhang, L., Li, H., Hu, X., Lu, L., Gong, Q., et al.: Impairments of large-scale functional networks in attention-deficit/hyperactivity disorder: a meta-analysis of resting-state functional connectivity. *Psychological medicine (2019)*
11. Greene, A.S., Shen, X., Noble, S., Horien, C., Hahn, C.A., Arora, J., Tokoglu, F., Spann, M.N., Carrión, C.I., Barron, D.S., et al.: Brain-phenotype models fail for individuals who defy sample stereotypes. *Nature (2022)*
12. Van der Hallen, R., Manning, C., Evers, K., Wagemans, J.: Global motion perception in autism spectrum disorder: a meta-analysis. *Journal of autism and developmental disorders (2019)*
13. Isakoglou, C., Haak, K.V., Wolfers, T., Floris, D.L., Llera, A., Oldehinkel, M., Forde, N.J., Oakley, B.F., Tillmann, J., Holt, R.J., et al.: Fine-grained topographic organization within somatosensory cortex during resting-state and emotional face-matching task and its association with asd traits. *Translational psychiatry (2023)*
14. Just, M.A., Cherkassky, V.L., Keller, T.A., Minshew, N.J.: Cortical activation and synchronization during sentence comprehension in high-functioning autism: evidence of underconnectivity. *Brain (2004)*

15. Kan, X., Dai, W., Cui, H., Zhang, Z., Guo, Y., Yang, C.: Brain network transformer. *Advances in Neural Information Processing Systems* (2022)
16. Lau, W.K., Leung, M.K., Lau, B.W.: Resting-state abnormalities in autism spectrum disorders: a meta-analysis. *Scientific reports* (2019)
17. Lopez-Larson, M.P., King, J.B., Terry, J., McGlade, E.C., Yurgelun-Todd, D.: Reduced insular volume in attention deficit hyperactivity disorder. *Psychiatry Research: Neuroimaging* (2012)
18. Loshchilov, I., Hutter, F.: Decoupled weight decay regularization. *International Conference on Learning Representations* (2019)
19. Luo, Y., Shi, M., Khan, M.O., Afzal, M.M., Huang, H., Yuan, S., Tian, Y., Song, L., Kouhana, A., Elze, T., Fang, Y., Wang, M.: Fairclip: Harnessing fairness in vision-language learning. *Conference on Computer Vision and Pattern Recognition* (2024)
20. Luo, Y., Tian, Y., Shi, M., Pasquale, L.R., Shen, L.Q., Zebardast, N., Elze, T., Wang, M.: Harvard glaucoma fairness: A retinal nerve disease dataset for fairness learning and fair identity normalization. *IEEE Trans. Medical Imaging* (2024)
21. Park, K., Oh, S., Kim, D., Kim, J.: Contrastive learning as a polarizer: Mitigating gender bias by fair and biased sentences. *Findings of the Association for Computational Linguistics: NAACL 2024* (2024)
22. Radford, A., Kim, J.W., Hallacy, C., Ramesh, A., Goh, G., Agarwal, S., Sastry, G., Askell, A., Mishkin, P., Clark, J., Krueger, G., Sutskever, I.: Learning transferable visual models from natural language supervision. *International Conference on Machine Learning* (2021)
23. Romani, M., Vigliante, M., Faedda, N., Rossetti, S., Pezzuti, L., Guidetti, V., Cardona, F.: Face memory and face recognition in children and adolescents with attention deficit hyperactivity disorder: A systematic review. *Neuroscience & Biobehavioral Reviews* (2018)
24. Samson, F., Mottron, L., Soulières, I., Zeffiro, T.A.: Enhanced visual functioning in autism: An ale meta-analysis. *Human brain mapping* (2012)
25. Vetter, N.C., Buse, J., Backhausen, L.L., Rubia, K., Smolka, M.N., Roessner, V.: Anterior insula hyperactivation in adhd when faced with distracting negative stimuli. *Human brain mapping* (2018)
26. Xiao, R., Kim, S., Georgescu, M.I., Akata, Z., Alaniz, S.: Flair: Vlm with fine-grained language-informed image representations (2024)
27. Xie, J., Girshick, R., Farhadi, A.: Unsupervised deep embedding for clustering analysis. *International conference on machine learning* (2016)
28. Yarkoni, T., Poldrack, R.A., Nichols, T.E., Van Essen, D.C., Wager, T.D.: Large-scale automated synthesis of human functional neuroimaging data. *Nature methods* (2011)
29. Zhai, X., Mustafa, B., Kolesnikov, A., Beyer, L.: Sigmoid loss for language image pre-training. *International Conference on Computer Vision* (2023)